


Equilibrium and dynamics of strained islandsGuido Schifani, Thomas Frisch,* and Médéric Argentina
Université Côte d'Azur, CNRS, INPHYNI, Nice, France (Received 24 July 2017; revised manuscript received 3 May 2018; published 29 June 2018)

We focus in this work on the effect of the surface energy anisotropy on an elastically strained semiconductor film and in particular on its role on the coarsening dynamics of elastically strained islands. To study the dynamics of a strained film, we establish a one-dimensional nonlinear and nonlocal partial differential equation which takes into account the elastic, capillary, wetting, and anisotropic effects. We first construct an approximate stationary solution of our model using a variational method and an appropriate ansatz. This stationary solution is used to compute the chemical potential dependence on the island height. In particular, we find that the surface energy anisotropy increases the convexity of the chemical potential and this is shown to have an effect on the driving force for the coarsening. Second, we study the coarsening dynamics of an islands pair by means of numerical simulations. We find that the presence of the surface energy anisotropy may increase or decrease the coarsening time of the system. We show that this phenomenon depends on the initial heights of island pairs. We thus highlight that the driving force for the coarsening is due to the variation of the chemical potential with respect to the islands height and that two different regimes are possible.

DOI: [10.1103/PhysRevE.97.062805](https://doi.org/10.1103/PhysRevE.97.062805)**I. INTRODUCTION**

The study of elastically strained semiconductor thin films is a challenging task from both theoretical and applied points of view [1–3]. The observation of self-organized strained islands appearing on semiconductor films has attracted a lot of interest due to their optoelectronic properties for light emitting diode and quantum dots laser [4–6]. The development of a model that explains the shape and the dynamics of strained islands (quantum dots) is a demanding and stimulating task, since it involves the dynamical interplay of elastic, capillary, wetting, and alloying effects [7–15].

As a semiconductor film is deposited on a substrate by heteroepitaxy, an elastic stress builds, because of the atomic lattice difference between the two semiconductors. The resulting mechanical stress can lead to a morphological instability [11,16–24]. This instability, known as the Asaro-Tiller-Grinfeld (ATG) instability [25,26], leads to the formation of parabolic-shaped islands (prepyramid) [27], which have been observed [20,21]. The prepyramids later evolve in pyramids as more material is deposited [27]. The control of these objects is of fundamental importance for applications, and the size selection of quantum dots is still under active research, mainly because the coarsening dynamics is complex to predict at nanoscales [10].

As shown in Refs. [10,11,28–30], self-organized strained islands display a coarsening dynamics which slows down and even lead to an interruption of the coarsening because of the surface energy anisotropy. In Ref. [29], the authors have exhibited a phenomenological model using an islands pair which permits to explain phenomenologically the slowing down of the coarsening induced by the presence of the surface energy

anisotropy. This work [29] makes use of an energetic model, which describes an energetic pathway along which ripening can indeed be frozen. However, there still remains several open questions such as the influence of the shape of the surface energy anisotropy on the rate of coarsening. Here we build on our previous work [32] in which we have proposed a simple ansatz for predicting the shape of an island under elastic strain, in quantitative agreement with numerical simulations. However, in Ref. [32], the surface energy anisotropy was not included and therefore no effect of its influences could be predicted. Furthermore, the model was isotropic, a limitation, since crystalline semiconductors are intrinsically anisotropic. Here we have improved our model [32], to take into account the effect of the surface energy anisotropy on the shape of an island and on the dynamics of an islands pair. We show that the coarsening time may increase or decrease when the surface energy anisotropy increases. This phenomenon depends on the islands pair height. We explain this effect by demonstrating that the surface energy anisotropy changes the convexity of the chemical potential, which plays an important role on the coarsening rate. The cause of the freezing of the coarsening induced by the surface energy anisotropy, as found in Ref. [29], remains an open question.

This article is constructed as follows: in Sec. II, we present a one-dimensional partial differential equation, nonlinear and nonlocal, which takes into account the anisotropy of surface energy, the elastic energy and the wetting effect. We then propose in Sec. III a parametric ansatz which minimises the energy of the system. This approach links the shape and the size of a single strained island to its height. We use this stationary solution to compute the variation of the chemical potential with respect to the island height. We find that the chemical potential convexity increases with the presence of the surface energy anisotropy. In Sec. IV, we study the coarsening dynamics of two islands under elastic strain. We find that the coarsening time depends on the surface anisotropy strength and on the

*thomas.frisch@inphyni.cnrs.fr

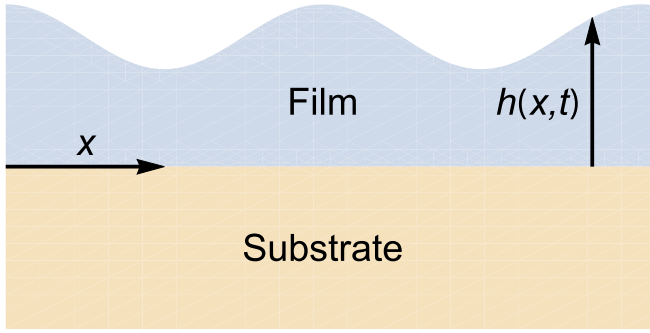


FIG. 1. Sketch of the system: $h(x,t)$ is the height of the free surface of the film with respect to the substrate.

initial islands heights, the coarsening time being accelerated for small islands and slowed down for large ones. This effect is displayed in Fig. 14.

II. CONTINUUM MODEL

Semiconductors film dynamics can be modeled by a mass conservation equation which takes into account the surface diffusion. The surface diffusion current is proportional to the gradient of the surface chemical potential μ . In the absence of evaporation, the 1D equation for the top surface of the film $h(x,t)$ reads

$$\frac{\partial h}{\partial t} = \mathcal{D} \sqrt{1 + h_x^2} \frac{\partial^2 \mu}{\partial s^2}, \quad (1)$$

where \mathcal{D} is the diffusion coefficient, $h_x(x,t) = \partial_x h(x,t)$ is the slope of the surface height, and ∂_s is the surface gradient [31,32] as shown in Fig. 1.

The chemical potential μ at the surface is defined by

$$\mu = \delta \mathcal{F} / \delta h. \quad (2)$$

Here \mathcal{F} is the free energy of the system, which takes into account the surface and the elastic contribution, noted \mathcal{F}_s and \mathcal{F}_{el} , respectively:

$$\mathcal{F} = \mathcal{F}_s + \mathcal{F}_{el}. \quad (3)$$

The chemical potential $\mu = \mu_s + \mu_{el} = \delta \mathcal{F}_s / \delta h + \delta \mathcal{F}_{el} / \delta h$ has thus a contribution from the surface energy and from the elastic energy. The surface energy per unit length reads

$$\mathcal{F}_s = \int \gamma(h, h_x) \sqrt{1 + h_x^2} dx, \quad (4)$$

where $\gamma(h, h_x)$ is the surface energy. It includes both wetting effects and surface energy anisotropy. As a first approximation, we examine a decomposition of the surface energy $\gamma(h, h_x)$, where the wetting and anisotropic effects are independent and may be written as

$$\gamma(h, h_x) = \gamma_f [1 + \gamma_w(h) + \gamma_a(h_x)]. \quad (5)$$

Here γ_f is the amplitude of the surface energy, $\gamma_w(h)$ is the wetting layer potential, and $\gamma_a(h_x)$ is a measure of the surface energy anisotropy. The wetting effects are linked to the film thickness h through the relation $\gamma_w(h) = c_w \exp(-h/\delta)$. The two parameters c_w and δ are, respectively, the amplitude and the range of the wetting potential [33].

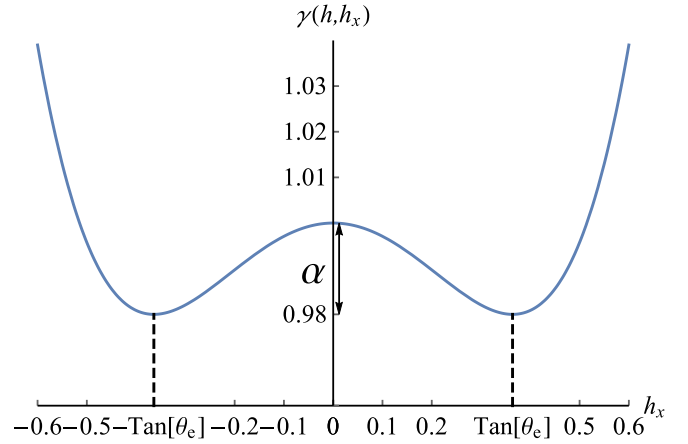


FIG. 2. Plot of the surface energy anisotropy $\gamma(h, h_x)/\gamma_f$ given in Eqs. (5) and (6) as a function of the slope h_x . The wetting layer potential $\gamma_w(h)$ having no dependence on h_x is not represented here. The anisotropy parameters are $\alpha = 0.01$ and $\theta_e = \pi/9$. The minimum of the surface energy is chosen at a value of $h_x = \pm \tan(\theta_e)$. The anisotropy strength α represents the amplitude of the perturbation. The vertical axis is in unit of γ_f .

We now assume for simplicity that the anisotropy term $\gamma_a(h_x)$ has only a single shallow minimum at a value $h_x = \pm \tan(\theta_e)$ and is an even function of h_x . The surface slope h_x is expected to be smaller than unity to be consistent with the small slope approximation [29]. The anisotropic contribution to surface energy is thus chosen to have the following form:

$$\gamma_a(h_x) = -\frac{2\alpha h_x^2}{\tan^2(\theta_e)} \left[1 - \frac{h_x^2}{2 \tan^2(\theta_e)} \right]. \quad (6)$$

As shown in Fig. 2, this type of anisotropy weakly favors an orientation with a slope $h_x = \pm \tan(\theta_e)$. Here α , which is a dimensionless quantity, represents the anisotropy strength as it measures the depth of the minimum as shown in Fig. 2. We plot in Fig. 3 the surface stiffness defined as $\tilde{\gamma} = \gamma(h, h_x) + \gamma''(h, h_x)$ for the isotropic ($\alpha = 0$) and anisotropic case ($\alpha \neq 0$); here the prime represents the derivatives with respect to h_x . The surface stiffness is always positive so this prevents any facetinglike instability. However, for small value of h_x the surface stiffness in the anisotropic case is smaller than the one in the isotropic case, while the opposite is true for large slope. As we will show later, this has a consequence on the dynamics of the coarsening.

To simplify Eq. (4), we can make use of the small slope approximation $h_x \ll 1$ and obtain the following equation for the surface energy:

$$\mathcal{F}_s = \gamma_f \int_{-L}^L \left[1 + \gamma_w(h) + \frac{1}{2} A(\alpha, \theta_e) h_x^2 + \frac{1}{12} B(\alpha, \theta_e) h_x^4 + \frac{1}{30} C(\alpha, \theta_e) h_x^6 \right] dx. \quad (7)$$

Here L represents the system size and the parameters $A(\alpha, \theta_e)$, $B(\alpha, \theta_e)$, and $C(\alpha, \theta_e)$ are found to be

$$A(\alpha, \theta_e) = 1 - 4\alpha \cot^2(\theta_e), \quad (8)$$

$$B(\alpha, \theta_e) = 12\alpha \cot^2(\theta_e) [\cot^2(\theta_e) - 1] - \frac{3}{2}, \quad (9)$$

$$C(\alpha, \theta_e) = \frac{15}{8} [8\alpha \cot^4(\theta_e) + 4\alpha \cot^2(\theta_e) + 1]. \quad (10)$$

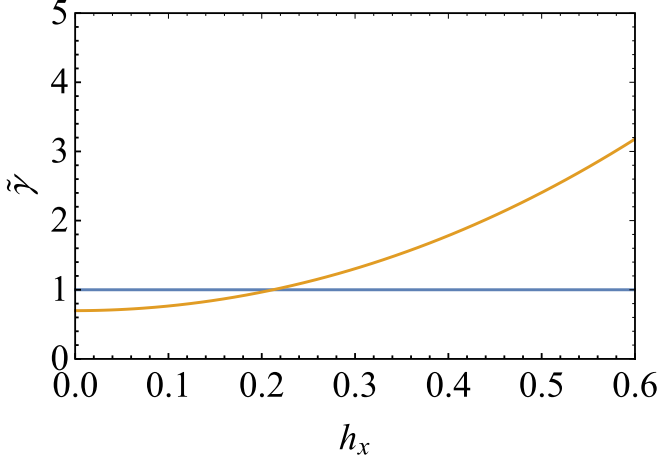


FIG. 3. Surface stiffness $\tilde{\gamma} = [\gamma(h, h_x) + \gamma''(h, h_x)]/\gamma_f$ obtained using Eqs. (5) and (6) as a function of h_x . The wetting layer potential $\gamma_w(h)$ having no dependence on h_x is not represented here. For $h_x < 0$ the surface stiffness is an even function of the slope h_x . The horizontal (blue color online) curve represents the surface stiffness for the isotropic case ($\alpha = 0$). The (orange color online) curve represents the stiffness for the anisotropic case ($\alpha = 0.01$ and $\theta_e = \pi/9$). The surface stiffness is always positive so that no missing orientations takes place. The vertical axis is in unit of γ_f .

Using Eqs. (2), (5), and (7), $\mu_s = \delta\mathcal{F}_s/\delta h$ reads

$$\mu_s = \gamma_f \left\{ [A(\alpha, \theta_e) + B(\alpha, \theta_e)h_x^2 + C(\alpha, \theta_e)h_x^4]h_{xx} - \frac{c_w}{\delta} e^{-h/\delta} \right\}. \quad (11)$$

The elastic energy per unit length is given by

$$\mathcal{F}_{el} = \mathcal{E}_0 \int_{-L}^L -\frac{h(x)\mathcal{H}[h_x(x)]}{2} dx. \quad (12)$$

Here the elastic energy density reads $\mathcal{E}_0 = Y\eta^2/(1-\nu)$. The parameter $\eta = (a_f - a_s)/a_s$ is the misfit parameter where a_f (respectively, a_s) is the film (respectively, substrate) lattice spacing, Y is the Young's modulus of the film and of the substrate, and ν the Poisson's coefficient. $\mathcal{H}[h_x(x)]$ is the Hilbert transform of the spatial derivative of $h(x, t)$. It can be defined as $\mathcal{H}[h_x] = \mathcal{F}^{-1}[|k|\mathcal{F}(h)]$, where \mathcal{F} is the Fourier transform and k is the wave number [34]. In real space, the Hilbert transform reads

$$\mathcal{H}[h_x] = \frac{1}{\pi} \int_{-L}^L \frac{h_y(y)}{x-y} dy. \quad (13)$$

The elastic chemical potential reads

$$\mu_{el} = -\mathcal{E}_0 \mathcal{H}[h_x]. \quad (14)$$

The evolution equation for the surface $h(x, t)$ merely follows from Eq. (1). With the small slope approximation, it reads

$$\frac{\partial h}{\partial t} = \mathcal{D} \frac{\partial^2(\mu_s + \mu_{el})}{\partial x^2}, \quad (15)$$

where μ_s and μ_{el} are given in Eqs. (11) and (14).

In the following, we choose l_0 for the unit of length of $h(x, t)$ and x , and t_0 for the unit of time. These are usual units (Refs. [29,32]). The length scale l_0 reads

$$l_0 = \gamma_f/\mathcal{E}_0. \quad (16)$$

It results from the balance of the typical surface energy γ_f with the elastic energy \mathcal{E}_0 density. The timescale t_0 reads

$$t_0 = l_0^4/(\mathcal{D}\gamma_f), \quad (17)$$

where \mathcal{D} is the surface diffusion coefficient [35]. From now on, all the variables will be written in dimensionless form.

Equation (15) is a nonlinear equation due to the presence of the nonlinear form of the wetting potential and of the surface energy anisotropy. Its dynamical evolution is dominated by a coarsening phenomenon, in which small islands disappear for the benefit of larger islands. As we will show in Sec. IV, when the system reaches equilibrium, only one island remains above the wetting layer. This island will be thus characterized by the parameters of the system, which are the two wetting constants c_w and δ , the two anisotropy constants α and θ_e , and the total surface of the system S_T , defined as

$$S_T = \int_{-L}^L h(x, t) dx. \quad (18)$$

The quantity S_T can be easily shown to be constant in time as a simple consequence of the conservative form of Eq. (15). The numerical integration of Eq. (15) is performed with a pseudospectral method on a periodic domain of size L which permits a simple implementation of the Hilbert transform [29,34].

III. EQUILIBRIUM CASE: ISLAND MORPHOLOGY

In this section, we first study the equilibrium shape of a single island. The island shape results from the balance between different effects such as the elastic stress field, the capillary effects (surface energy anisotropy), and the wetting effect. Moreover, the parameter S_T plays an important role since it is directly related to the spatial mean of the surface height by the relation $S_T = \langle h \rangle L$. We investigate the shape of an island for different values of the control parameters S_T and α .

Using a variational method, we determine the characteristic parameters of the island, such as its size and chemical potential, as a function of the island height and of the anisotropy parameter α . Our approach consists in the minimization of the total energy of the system using a simple ansatz which takes into account the constraint of constant surface S_T .

An approximation of the stationary island solution $h(x)$ can be obtained by the minimisation of the energy given in Eq. (3) using a simple ansatz. This ansatz for the surface $h(x)$ is

$$h(x) = \begin{cases} h_w & -L < x < -x_1, \\ h_{in}(x) = h_0 + bx^2 + cx^4 + dx^6 & -x_1 \leq x \leq x_1, \\ h_w & x_1 < x < L. \end{cases} \quad (19)$$

This ansatz is composed of two parts. A center part, $h_{in}(x)$ of horizontal extent x_1 , which is described by a polynomial that presents a maximum height h_0 at $x = 0$ (see Fig. 4). An outer part, for $|x| > x_1$, which describes the wetting layer of constant height h_w . The center part $h_{in}(x)$ requires the determination of five parameters x_1, h_0, b, c, d . Therefore, we will need five conditions to determine the five unknown parameters.

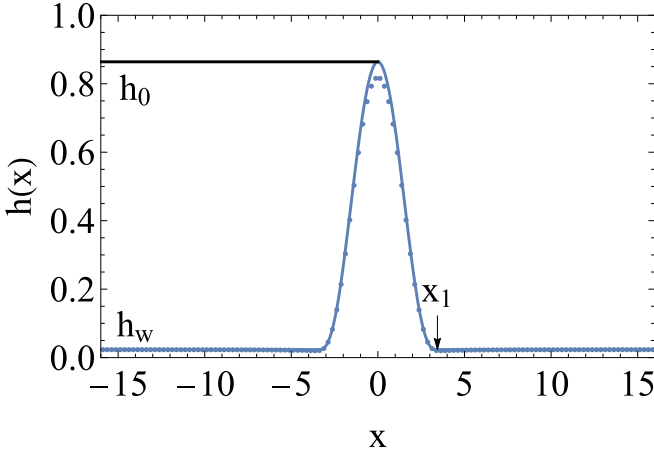


FIG. 4. Stationary solutions obtained by the numerical simulation of Eq. (15) (dots) compared to the ansatz proposed in Eq. (23) (continuous curve) for the isotropic case $\alpha = 0$. The height of the island is represented by h_0 , the height of the wetting layer is represented by h_w and x_1 is the half-width of the island. The initial condition is given by a small random perturbation around a constant value of $h = 0.1$. The value of the surface is $S_T = 3.25$. We use as wetting parameters $c_w = 0.05$ and $\delta = 0.005$. The system size is $L = 16$. The horizontal and vertical axes are in units of l_0 .

First of all, the chemical potential depends on the first and second derivatives of the free surface $h(x,t)$, therefore we impose the continuity of $h(x,t)$, $\partial_x h(x,t)$, and $\partial_{xx} h(x,t)$ at $x = x_1$. This leads to the following three conditions:

$$h_{\text{in}}(x_1) = h_w, \quad (20)$$

$$\mathcal{F}_{el} = -\frac{32(8h_0 - 3h_w)(h_0 - h_w)}{150\pi} + \frac{2h_w(h_0 - h_w)[-15L^5x_1 + 40L^3x_1^3 + 15(L^2 - x_1^2)^3 \tanh^{-1}\left(\frac{x_1}{L}\right) - 33Lx_1^5 + 8x_1^6]}{15\pi x_1^6}. \quad (26)$$

Here \mathcal{F}_{el} is also a dimensionless quantity and is expressed in units of $\frac{\gamma_f^2}{\mathcal{E}_0} = \mathcal{E}_0 l_0^2$.

Similarly, it can be shown using Eq. (23) that the surface energy contributions \mathcal{F}_s reads

$$\begin{aligned} \mathcal{F}_s = & \frac{a_s(h_0 - h_w)^6(8\alpha \cot^4(\theta_e) + 4\alpha \cot^2(\theta_e) + 1)}{x_1^5} \\ & + \frac{b_s(h_0 - h_w)^4(8\alpha \cot^4(\theta_e) - 8\alpha \cot^2(\theta_e) - 1)}{x_1^3} \\ & - \frac{c_s(h_0 - h_w)^2(4\alpha \cot^2(\theta_e) - 1)}{x_1} \\ & + 2(L - x_1)\left(1 + c_w e^{-\frac{h_w}{\delta}}\right) + 2x_1, \end{aligned} \quad (27)$$

where a_s , b_s , and c_s have the value defined in Ref. [36]. Here \mathcal{F}_s is also a dimensionless quantity and is expressed in units of $\frac{\gamma_f^2}{\mathcal{E}_0} = \gamma_f l_0$. We have neglected the contribution of the wetting effect in the island region ($-x_1 < x < x_1$) because of the exponential decay of the wetting potential with the height $h(x,t)$.

$$\partial_x h_{\text{in}}(x)|_{x=x_1} = 0, \quad (21)$$

$$\partial_{xx} h_{\text{in}}(x)|_{x=x_1} = 0. \quad (22)$$

The three unknown parameters b , c , and d can be found by solving the linear system of Eqs. (20), (21), and (22). We thus obtain

$$h(x) = \begin{cases} h_w & -L < x < -x_1, \\ h_{\text{in}}(x) = (h_0 - h_w) \frac{(x_1^2 - x^2)^3}{x_1^6} + h_w & -x_1 \leq x \leq x_1, \\ h_w & x_1 < x < L. \end{cases} \quad (23)$$

Finally there remains only two unknowns which are the island width x_1 and the island height h_0 as described in Fig 4. These two parameters can be found by the minimization of the energy $\mathcal{F} = \mathcal{F}_s + \mathcal{F}_{el}$ defined in Eqs. (7) and (12). This minimization is done by taking into account the constraint of fixed surface S_T .

A simple analysis of Eqs. (18) and (23) shows that the surface S_T reads

$$S_T = \frac{32h_0x_1}{35} + 2h_w(L - x_1) + \frac{38h_wx_1}{35}. \quad (24)$$

We can easily invert Eq. (24) and express h_w as a function of S_T , it reads

$$h_w = \frac{35S_T - 32h_0x_1}{2(35L - 16x_1)}. \quad (25)$$

Using Eq. (23), we find that the elastic energy given in Eq. (12) reads

The total energy $\mathcal{F} = \mathcal{F}_{el} + \mathcal{F}_s$ is thus a function of h_0 and of x_1 . The value of h_0 and x_1 are now determined by the two minimizing conditions:

$$\frac{\partial \mathcal{F}}{\partial h_0} = 0, \quad (28)$$

$$\frac{\partial \mathcal{F}}{\partial x_1} = 0. \quad (29)$$

Equations (28) and (29) are two nonlinear transcendental equations for the unknowns h_0 and x_1 . These equations can be numerically solved using a simple root finding algorithm and yield the island height h_0 and the island width x_1 as a function of the total surface S_T . As shown in Fig. 5, the energy landscape of \mathcal{F} as a function of h_0 and x_1 displays a well defined minimum.

To validate our assumptions and predictions, we have performed numerical simulation of Eq. (15) using a pseudo-spectral method as used in Ref. [32]. Our predictions, compared to our numerical simulations, are shown in Figs. 6–10. The numerical simulations are performed with an initial constant mean height $\langle h \rangle$ perturbed by a small random initial

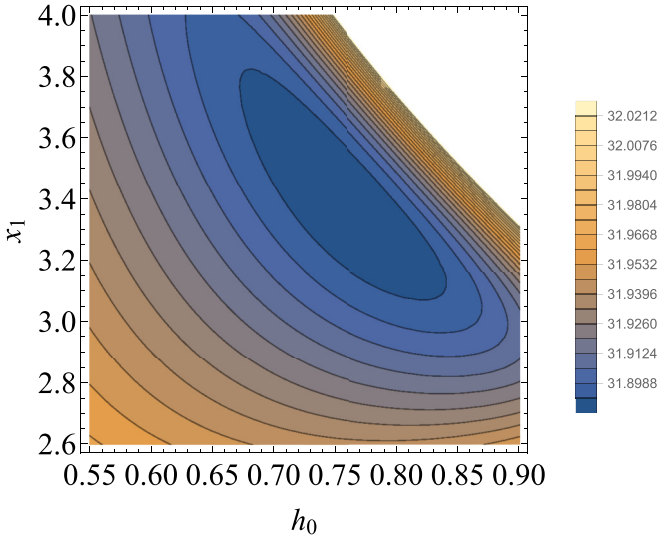


FIG. 5. Energy of the system given in Eq. (3) as a function of the island height h_0 and the island width x_1 . The wetting parameters are $c_w = 0.05$ and $\delta = 0.005$, and the anisotropic parameters are $\alpha = 0.01$ and $\theta_e = \pi/9$. The system size is $L = 16$ and the total surface is $S_T = 3$. The horizontal and vertical axes are in units of l_0 . The energy is in unit of γ_f^2/\mathcal{E}_0 .

noise. The mean height $\langle h \rangle$ is related to the total surface (mass) given in Eq. (18) by the relation $S_T = \langle h \rangle L$. In our numerical simulation, we vary the initial mean height $\langle h \rangle$ (or S_T) and the anisotropy strength α .

First, we study the isotropic case, $\alpha = 0$. We plot in Fig. 6 various islands profiles obtained by numerical simulation of Eq. (15) for different values of the surface S_T . We find a good agreement between the numerical simulation and our analytical predictions given by the solution of Eqs. (28) and (29) for the island half-width x_1 as a function of the island height h_0 . Moreover for $\alpha = 0$, as shown in the Fig. 6 inset, we have found that for small island height h_0 , the island half-width x_1 is nearly constant around the value $x_1 = 9\pi/8$, as found in Ref. [32].

We now analyze the effect of the anisotropy α on the island shape. We choose a value of $\alpha = 0.01$ and a preferential angle $\theta_e = \pi/9$. We plot in Fig. 7 various islands profiles obtained by numerical simulation for different values of surface S_T . We first observe that for small island height h_0 , the half-width x_1 in the anisotropic case is smaller than in the isotropic case. This is due to the fact that the surface stiffness $\tilde{\gamma} = \gamma + \gamma''$ is smaller for the anisotropic case (see Fig. 3). The behavior of the anisotropic island half-width x_1 as a function of the island height h_0 is shown in the Fig. 7 inset. The island width x_1 increases with respect to the island height h_0 . This is a consequence of the surface energy anisotropy which favors an island slope $h_x = \tan(\theta_e)$. We obtain a good agreement between the analytical solution given in Eqs. (28) and (29) and our numerical simulations.

Moreover, we determine numerically the chemical potential of an island as a function of the island height h_0 for the isotropic case ($\alpha = 0$) and anisotropic case ($\alpha = 0.01$), using the equilibrium numerical solution of Eq. (15). For a stationary

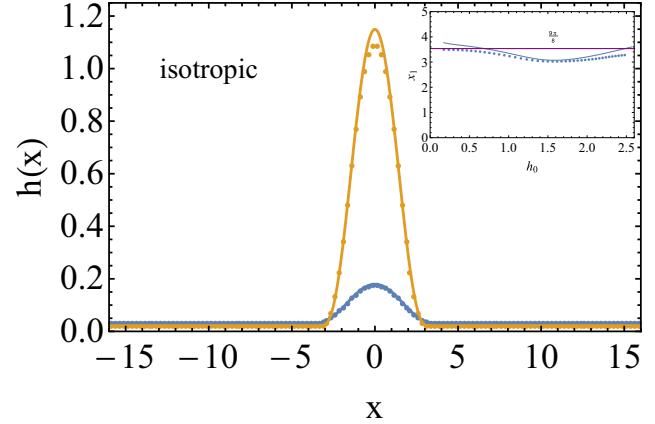


FIG. 6. Isotropic case: $\alpha = 0$, x_1 is the half-width of the island is almost constant with respect to h_0 . Blue-curve bottom ($S_T = 1.5$), orange ($S_T = 3.9$), color online. The islandlike solutions (dots) resulting from the numerical simulations of Eq. (15) are compared to the ansatz proposed in Eq. (23) represented by the continuous curve. The wetting parameters are $c_w = 0.05$ and $\delta = 0.005$, the system size is $L = 16$. The horizontal and vertical axes are in units of l_0 . Inset: Island half-width x_1 as a function of the island height h_0 for the isotropic case ($\alpha = 0$). The blue dots represents the numerical results of Eq. (15) surface value between $S_T = 1.45$ and $S_T = 8.21$. The solid blue curve is the prediction obtained using Eqs. (28) and (29) for the island half-width x_1 . The straight line $x_1 = \frac{9\pi}{8}$ is the value obtained in Ref. [32] in which we have used a linear approximation of the film curvature. The horizontal and vertical axes are in units of l_0 .

profile of Eq. (15), the chemical potential μ is equal to

$$\mu = -\frac{c_w}{\delta} e^{-h_w/\delta}, \quad (30)$$

where we have assumed that far from the island the film is flat, and the wetting layer height is equal to h_w , as shown in Fig. 4. As a consequence, the terms h_x and h_{xx} can be neglected and only the wetting potential term remains dominant in Eqs. (11) and (14). As shown in Fig. 8, the chemical potential μ decays as a function of the island height h_0 and its convexity increases with the anisotropy strength α . The decay of the chemical potential μ as a function of the height is mostly due to the relaxation effect of elasticity. The increase of the convexity of the chemical potential with the anisotropy strength α is explained by the dominance of the surface energy anisotropy which favors the slope of the island $\tan(\theta_e) = \pi/9$. As a consequence of this convexity, we can foresee that the coarsening rate will decrease when the island height is large enough. As we have shown previously [32], the coarsening rate is proportional to the mass transfer between the islands. This mass transfer is driven by the difference of the chemical potential between the islands. As the convexity increases, the slope of the chemical potential μ decreases, and therefore the difference in the chemical potential between the island decreases. However, for small island height, the slope of the chemical potential μ with respect to h_0 is larger when the anisotropy strength is increased, and we thus expect an acceleration of the coarsening.

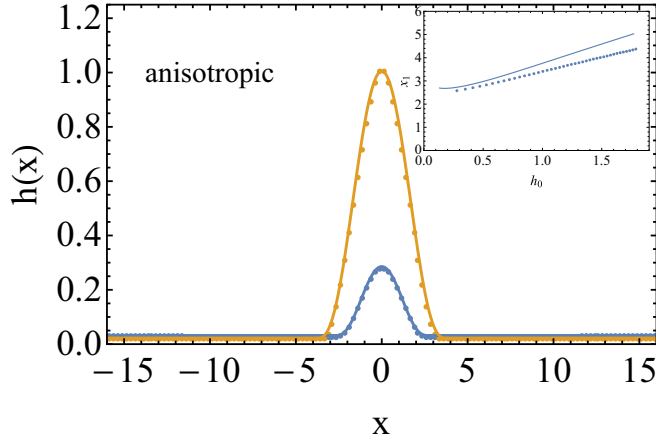


FIG. 7. Anisotropic case: x_1 increases with respect to h_0 . Islandlike solutions resulting from the time evolution of Eq. (15). Numerical simulations of Eq. (15) represented by dots, compared to the ansatz proposed in Eq. (23) represented by the continuous curve. We use as wetting parameters $c_w = 0.05$ and $\delta = 0.005$. The anisotropic strength is $\alpha = 0.01$ and $\theta_e = \pi/9$. The system size is $L = 16$. From bottom to top: blue-curve bottom ($S_T = 1.5$), orange ($S_T = 3.9$), color online. The horizontal and vertical axes are in units of l_0 . Inset: Island half-width x_1 as a function of the island height h_0 for the anisotropic case ($\alpha = 0.01$ and $\theta_e = \pi/9$). The results of the numerical results of Eq. (15) are represented by dots for different values of the surface. The surface varies from a value of $S_T = 1.45$ to a value of $S_T = 8.21$. The solid curve is the prediction obtained using Eqs. (28) and (29) for the island half-width x_1 . The horizontal and vertical axes are in units of l_0 .

As shown in Fig. 9, the derivative of the chemical potential with respect to the island height, which represents the driving force for coarsening, is larger for island height value which are smaller than a critical value h_c . This critical value of h_c depends on α . This will have a consequence on the coarsening dynamics as we will show in the next section. We compare the island height h_0 for the isotropic case ($\alpha = 0$) and anisotropic case ($\alpha = 0.01$) as a function of the surface S_T . In Fig. 10, we observe that in the anisotropic case, for small amount of surface S_T , the island height h_0 is larger than in the isotropic case. However, for large surface S_T , the island height h_0 is larger in the isotropic case. The agreement between the numerical simulation and the variational method is again satisfactory.

IV. COARSENING DYNAMICS OF TWO ISLANDS

In this section, we characterize the coarsening of two islands and we study the influence of the anisotropy on the coarsening time. We define the coarsening time t_c to be the characteristic time for the system to reach equilibrium. After this time, the system is in equilibrium and only one island remains in the system. For practical matter, we choose to define t_c as the time at which the height of the remaining island has reached 99% of its final value. To study the coarsening dynamics, we choose for simplicity to start with an initial condition composed of two equilibrium islands with slightly different heights $h_1(0)$ and $h_2(0)$. The islands are separated by a distance d , which for simplicity is half of the system size $d = L/2$.

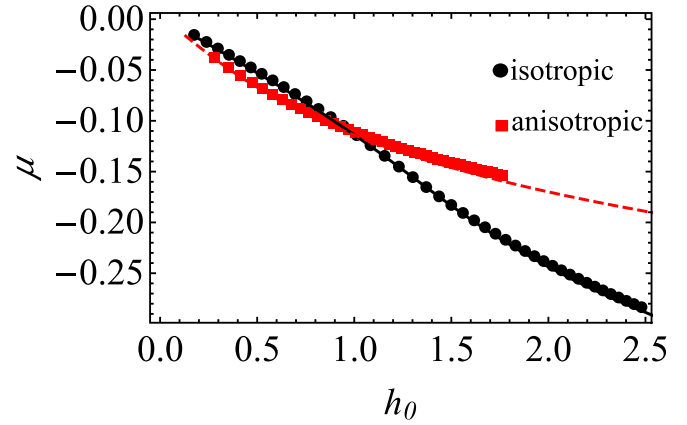


FIG. 8. Chemical potential μ as a function of the island height h_0 for the isotropic and anisotropic case. The black dots are obtained by the numerical simulations of Eq. (15) for $\alpha = 0$ and the red squares are obtained by the numerical simulations for $\alpha = 0.01$. The continuous black curve and the red dashed curve are obtained using the analytical predictions of Eqs. (28)–(30), respectively, for $\alpha = 0$ and $\alpha = 0.01$. As shown in this figure, the convexity of the chemical potential is larger for $\alpha = 0.01$ (red curve) than for $\alpha = 0$ (black curve). The value of the preferential slope is $\theta_e = \pi/9$. The horizontal axis is in units of l_0 and the vertical axis is in units of γ_f .

We perform numerical simulations for two different values of initial total surface S_T ($S_T = 2.91$ and $S_T = 4.15$), and five different values of the anisotropy strength α ($\alpha = 0$, $\alpha = 0.0025$, $\alpha = 0.005$, $\alpha = 0.0075$, and $\alpha = 0.01$). Our numerical simulations presented in Fig. 11 reveals that during the coarsening the larger island increases at expense of the smaller island until it disappears. Ultimately for $t > t_c$, only one island

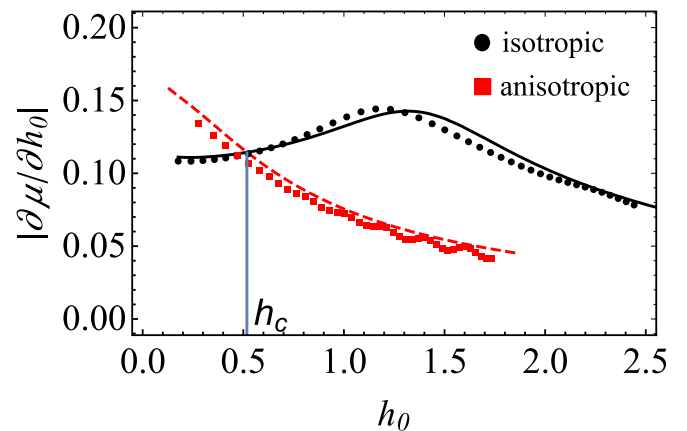


FIG. 9. Coarsening driving force: absolute value of the derivative of the chemical potential μ with respect to the island height h_0 . The black disks and the red squares are obtained respectively from the numerical simulations of Eq. (15) for $\alpha = 0$ and $\alpha = 0.01$. The continuous black curve ($\alpha = 0$) and the red dashed curve ($\alpha = 0.01$) are obtained using Eqs. (28)–(30). The critical height h_c is defined as the point at which the black curve and the red dashed curve intersect. At this point h_c , the two tangents to the the curves displayed on Fig. 8, have the same slope. The value of the preferential slope is $\theta_e = \pi/9$. The horizontal axis is in units of l_0 and the vertical axis is in units of γ_f .

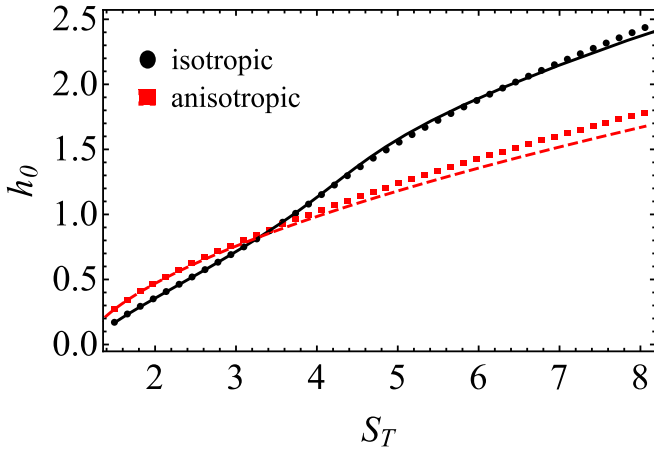


FIG. 10. Island height h_0 as a function of the surface S_T . The black dots and the red squares represent, respectively, the results of the numerical simulations of Eq. (15) for $\alpha = 0$ and $\alpha = 0.01$. The black solid curve ($\alpha = 0$) and the red dashed curve ($\alpha = 0.01$) are obtained using the resolution of Eqs. (24), (28), and (29). The system size is $L = 16$ for all the simulations. The horizontal axis is in units of l_0^2 and the vertical axis is in units of l_0 .

remains in the system. We present the time evolution of the heights $h_1(t)$ and $h_2(t)$ of two islands obtained by the numerical simulations of Eq. (15) for two regimes (small islands and large islands). In Fig. 12 the island heights are small, whereas in Fig. 13 the island heights are large.

The previous results shown on Figs. 12 and 13 on the coarsening time shows that depending on the island height coarsening can be slowed down or accelerated and that this phenomenon depends on the islands pair height.

In Fig. 14, we show that for large islands, the coarsening time increases with the anisotropy, while the anisotropy reduces the coarsening time for small islands. We propose

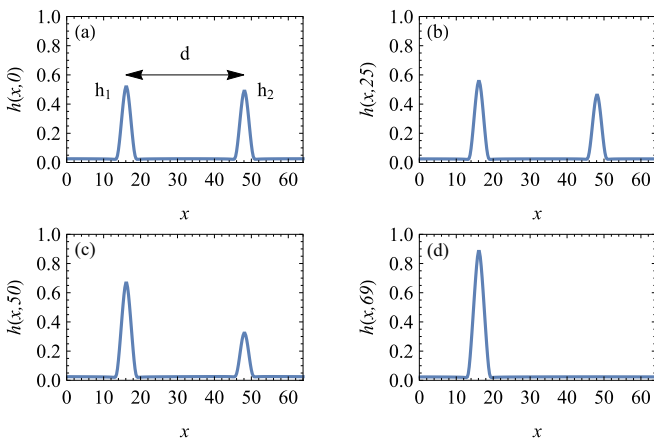


FIG. 11. Spatiotemporal evolution of two islands computed by the numerical simulation of Eq. (15). The initial condition are two islands of height $h_1 = 0.51$ and $h_2 = 0.49$ separated by a distance $d = L/2$, where $L = 64$ represents the system size. The anisotropic parameters are $\alpha = 0.01$ and $\theta = \pi/9$. After a time $t_c = 69$, only one island remains in the system. The horizontal and vertical axes are in units of l_0 .

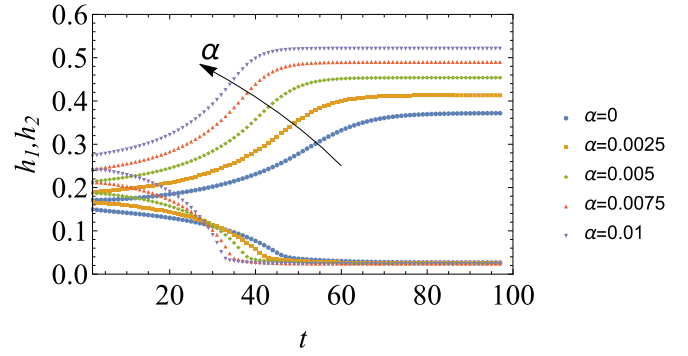


FIG. 12. Time evolution of the islands heights $h_1(t)$ and $h_2(t)$. We perform five numerical simulations of Eq. (15) for different values of the anisotropy strength α (blue dot $\alpha = 0$, orange square $\alpha = 0.0025$, green rhombus $\alpha = 0.005$, red up-pointing triangle $\alpha = 0.0075$, and violet down-pointing triangle $\alpha = 0.01$). We observe that as the anisotropy increases, the coarsening time decreases. The initial system surface is $S_T = 2.91$ for the five numerical simulations. The horizontal axis is in units of t_0 and the vertical axis is in units of l_0 .

here a simple argument which explains this nonintuitive effect. The driving force for coarsening $|\frac{\partial\mu}{\partial h}|$ is proportional to the difference of the chemical potential between the two islands. For small islands (smaller than h_c as defined on Fig. 9), the driving force for coarsening is larger in the anisotropic case ($|\partial\mu/\partial h_0|_{\alpha=0} < |\partial\mu/\partial h_0|_{\alpha\neq 0}$), as shown in Fig. 9. On the contrary, for large islands (larger than h_c), the driving force for coarsening is smaller in the anisotropic case ($|\partial\mu/\partial h_0|_{\alpha\neq 0} < |\partial\mu/\partial h_0|_{\alpha=0}$), as shown in Fig. 9. These effects can be explained by the convexity of the chemical potential μ , which increases with the anisotropy strength α , as shown in Fig. 8. The boundary between these two regimes (small islands and large islands) is the point at which the two tangents to the curve $\mu(h_0)$ on Fig. 8 have the same slope and is approximately equal to be $h_c = 0.5$. Equivalently, h_c is defined at the point at which the driving force for coarsening $|\partial\mu/\partial h|$ has the same value in the isotropic and anisotropic case as shown in Fig. 9. To conclude

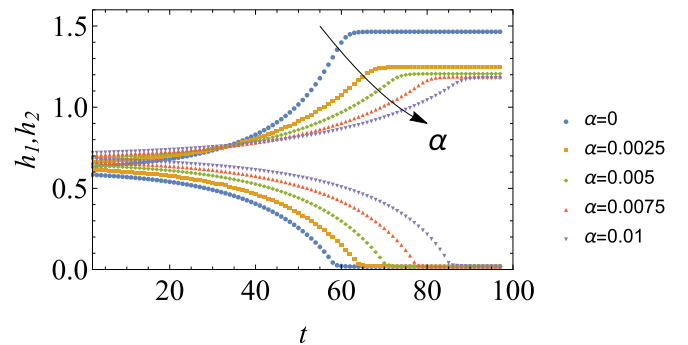


FIG. 13. Time evolution of the island heights $h_1(t)$ and $h_2(t)$. We perform five numerical simulations of Eq. (15) for different values of the anisotropy strength α (blue dot $\alpha = 0$, orange square $\alpha = 0.0025$, green rhombus $\alpha = 0.005$, red up-pointing triangle $\alpha = 0.0075$, and violet down-pointing triangle $\alpha = 0.01$). We observe that as the anisotropy increases, the coarsening time increases. The initial system surface is $S_T = 4.15$ for the five numerical simulations. The horizontal axis is in units of t_0 and the vertical axis is in units of l_0 .

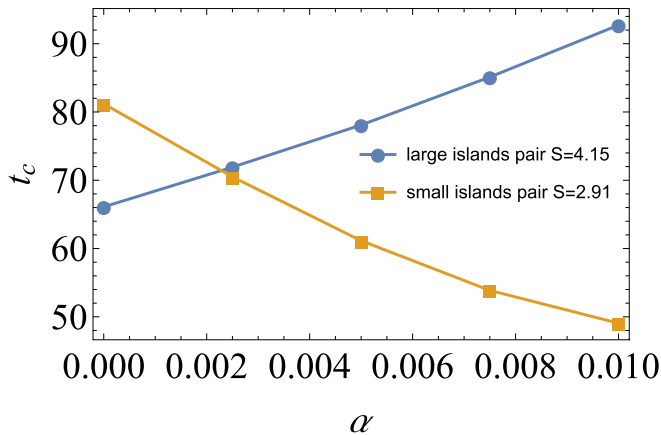


FIG. 14. Coarsening time t_c as a function of the anisotropy strength α for two different values of S_T . The system under study consists of two islands similar to the one shown in Fig. 11. The decreasing curve (orange square) is obtained using the numerical simulations of Eq. (15) for $S_T = 2.91$ (small islands). The blue curve (blue disk) is obtained using the numerical simulations of Eq. (15) for $S_T = 4.15$ (large islands). The vertical axis is in units of t_0 .

this section, let us note that the functional dependence of h_c on α can be obtained using the tools that we have presented in this article. In particular, we conjecture that the scaling behavior of t_c versus h_0 for a fixed value of α should exhibit two different scaling regimes in h_0 separated by a crossover at h_c . A natural extension of this work could be realized in three dimensional system for which coarsening phenomena has been shown to be very sensitive to the functional form of the surface energy anisotropy. In particular, the strong slowing down of coarsening predicted and observed in Refs. [10,29] still requires a more deeper mathematical analysis. In particular, we believe that the results obtained in Refs. [10,29] were found in the regime of large islands heights in which coarsening is slowed down.

V. CONCLUSION

This article presents an analytical and a numerical study of the morphology and of the dynamics of strained semiconductor islands in the presence of a surface energy anisotropy. Using a simple model, we have found that the anisotropy accelerates the coarsening time for small islands while it slows down the

coarsening for large islands. In the first part of this article, we have shown that the main morphological feature of an island can be described by a simple ansatz whose parameters are determined by a variational method. This method permits us to compute the island shape and its chemical potential as a function of its height. Moreover, we have found that the presence of the surface energy anisotropy increases the convexity of the chemical potential of an island and this phenomena affects the driving force for coarsening. In the second part of this article, we have performed numerical simulations of the coarsening dynamics of two islands using the model introduced in the first part. We have shown numerically that the coarsening time can increase or decrease depending on the values of the island height. This effect is attributed to the change of the driving force for coarsening induced by the convexity of the chemical potential. An extension of this work for a three-dimensional system could reveal a different behavior. The N-island problem is much more complex to handle from a purely theoretical point of view since it is a N-body problem with long-range elastic interactions, which could be solved within a mean field theory framework [22]. We believe that the islands pair problem could be a good starting point for the elaboration of a model of N interacting islands. Clearly, the two possible scenarios predicted for an islands pair will have consequence in the dynamics of a large number of islands. Furthermore, we have proposed a generic form for the surface energy anisotropy. It would be of interest to develop a similar approach for faceted systems which could explain quantitatively the freezing of the coarsening observed in Ref. [11]. In particular, the study of the freezing of the coarsening as a function of the system parameters, such as the shape around the surface anisotropy energy minimum (depth and radius of curvature), should be interesting. Finally, it seems possible that the results we have predicted for an islands pair could be compared with experiments in semiconductor islands (SiGe and AlGaIn quantum dots) with a low surface density of pairs [37].

ACKNOWLEDGMENTS

We thank Franck Celestini, Jean-Noël Aqua, Isabelle Berbezier, Pierre Müller, and Julien Brault for useful discussions. We thank the ANR NanoGanUV for financial support (Grant No. ANR-14-CE26-0025-01).

-
- [1] A. Pimpinelli and J. Villain, *Physics of Crystal Growth*, Collection Alea-Saclay: Monographs and Texts in Statistical Physics (Cambridge University Press, Cambridge, 1998).
 - [2] P. Politi, G. Grenet, A. Marty, A. Ponchet, and J. Villain, *Phys. Rep.* **324**, 271 (2000).
 - [3] J. E. Ayers, *Heteroepitaxy of Semiconductors: Theory, Growth, and Characterization* (CRC Press, Boca Raton, FL, 2007).
 - [4] V. A. Shchukin and D. Bimberg, *Rev. Mod. Phys.* **71**, 1125 (1999).
 - [5] J. Stangl, V. Holý, and G. Bauer, *Rev. Mod. Phys.* **76**, 725 (2004).
 - [6] J. Brault, S. Matta, T.-H. Ngo, D. Rosales, M. Leroux, B. Damianno, M. A. Khalfioui, F. Tendille, S. Chenot, P. D. Mierry *et al.*, *Mater. Sci. Semicond. Process.* **55**, 95 (2016).
 - [7] B. J. Spencer, P. W. Voorhees, and S. H. Davis, *Phys. Rev. Lett.* **67**, 3696 (1991).
 - [8] P. Müller and A. Saúl, *Surf. Sci. Rep.* **54**, 157 (2004).
 - [9] C.-H. Chiu and Z. Huang, *Appl. Phys. Lett.* **89**, 171904 (2006).
 - [10] J.-N. Aqua, A. Gouy e, A. Ronda, T. Frisch, and I. Berbezier, *Phys. Rev. Lett.* **110**, 096101 (2013).

- [11] J.-N. Aqua, I. Berbezier, L. Favre, T. Frisch, and A. Ronda, *Phys. Rep.* **522**, 59 (2013).
- [12] B. J. Spencer and J. Tersoff, *Phys. Rev. B* **87**, 161301 (2013).
- [13] C. Wei and B. J. Spencer, *Proc. Math. Phys. Eng. Sci.* **472**, 2190 (2016).
- [14] F. Rovaris, R. Bergamaschini, and F. Montalenti, *Phys. Rev. B* **94**, 205304 (2016).
- [15] C. Wei and B. J. Spencer, *Proc. Math. Phys. Eng. Sci.* **473**, 2206 (2017).
- [16] D. Srolovitz, *Acta Metall.* **37**, 621 (1989).
- [17] Y.-W. Mo, D. E. Savage, B. S. Swartzentruber, and M. G. Lagally, *Phys. Rev. Lett.* **65**, 1020 (1990).
- [18] D. J. Eaglesham and M. Cerullo, *Phys. Rev. Lett.* **64**, 1943 (1990).
- [19] J. A. Floro, E. Chason, L. B. Freund, R. D. Twisten, R. Q. Hwang, and G. A. Lucadamo, *Phys. Rev. B* **59**, 1990 (1999).
- [20] P. Sutter and M. G. Lagally, *Phys. Rev. Lett.* **84**, 4637 (2000).
- [21] R. M. Tromp, F. M. Ross, and M. C. Reuter, *Phys. Rev. Lett.* **84**, 4641 (2000).
- [22] J. A. Floro, M. B. Sinclair, E. Chason, L. B. Freund, R. D. Twisten, R. Q. Hwang, and G. A. Lucadamo, *Phys. Rev. Lett.* **84**, 701 (2000).
- [23] I. Berbezier and A. Ronda, *Surf. Sci. Rep.* **64**, 47 (2009).
- [24] C. Misbah, O. Pierre-Louis, and Y. Saito, *Rev. Mod. Phys.* **82**, 981 (2010).
- [25] R. J. Asaro and W. A. Tiller, *Metall. Trans.* **3**, 1789 (1972).
- [26] M. A. Grinfeld, *Sov. Phys. Dokl.* **31**, 831 (1986).
- [27] J. Tersoff, B. J. Spencer, A. Rastelli, and H. von Känel, *Phys. Rev. Lett.* **89**, 196104 (2002).
- [28] Y. W. Zhang, *Phys. Rev. B* **61**, 10388 (2000).
- [29] J.-N. Aqua and T. Frisch, *Phys. Rev. B* **82**, 085322 (2010).
- [30] M. Korzec and P. Evans, *Physica D: Nonlin. Phenom.* **239**, 465 (2010).
- [31] M. S. Levine, A. A. Golovin, S. H. Davis, and P. W. Voorhees, *Phys. Rev. B* **75**, 205312 (2007).
- [32] G. Schifani, T. Frisch, M. Argentina, and J.-N. Aqua, *Phys. Rev. E* **94**, 042808 (2016).
- [33] P. Müller and R. Kern, *Appl. Surf. Sci.* **102**, 6 (1996).
- [34] J.-N. Aqua, T. Frisch, and A. Verga, *Phys. Rev. B* **76**, 165319 (2007).
- [35] For example, for a $\text{Si}_{0.75}\text{Ge}_{0.25}$ film on Si, we find $l_0 = 27$ nm, and $t_0 = 23$ s at 700°C (see Ref. [19] for an estimate of surface diffusion coefficients).
- [36] $a_s = \frac{2717908992}{3038795305}$, $b_s = \frac{1179648}{1616615}$, and $c_s = \frac{512}{385}$.
- [37] Isabelle Berbezier and Julien Brault (private communication).